

Discovery of Millisecond Variability in the Neutron-Star X-Ray Transient SAX J1750.8-2900

P. Kaaret

Harvard-Smithsonian Center for Astrophysics, 60 Garden St., Cambridge, MA 02138, USA
 pkaaret@cfa.harvard.edu

J.J.M. in 't Zand

Astronomical Institute, Utrecht University, P.O. Box 80 000, 3508 TA Utrecht, the Netherlands
SRON National Institute for Space Research, Sorbonnelaan 2, 3584 CA Utrecht, the Netherlands

J. Heise

SRON National Institute for Space Research, Sorbonnelaan 2, 3584 CA Utrecht, the Netherlands

J.A. Tomsick

*Center for Astrophysics and Space Sciences, Code 0424, 9500 Gilman Drive,
 University of California at San Diego, La Jolla, CA 92093*

ABSTRACT

We report the discovery of millisecond oscillations in the X-ray emission from the X-ray transient SAX J1750.8-2900. Millisecond quasiperiodic oscillations (kHz QPOs) were present in the persistent emission with frequencies ranging from 543 Hz to 1017 Hz. Oscillations at a frequency of 600.75 Hz were present in the brightest X-ray burst observed. We derive an upper limit on the source distance of 6.3 ± 0.7 kpc from this X-ray burst.

Subject headings: accretion, accretion disks — gravitation — relativity — stars: individual (SAX J1750.8-2900) — stars: neutron — X-rays: stars

1. Introduction

The discovery of millisecond oscillations in the persistent emission and also in thermonuclear X-ray bursts from neutron star low-mass X-ray binaries (LMXBs) has opened a new window on the dynamics of accreting neutron stars (Strohmayer et al. 1996). The time scales of the kHz quasiperiodic oscillations found in the persistent emission (hereafter kHz QPOs) match those expected from accretion dynamics very close to the neutron star in a region of strong gravity, and the possibility that the kHz QPOs could be used as probes of strong gravity is very intriguing. The burst oscillations are in a range expected for the neutron star spin

periods (Alpar & Shaham 1985), and have been interpreted as evidence for millisecond spin periods in accreting neutron stars (Strohmayer et al. 1997). However, this interpretation has recently been questioned because of the large frequency shifts seen in some bursts. Observations of bursts from new sources would be useful in determining the correct interpretation of the burst oscillations.

Here, we describe observations made with the Rossi X-Ray Timing Explorer (RXTE; Bradt, Rothschild, & Swank 1993) following the detection of X-ray bursts from the transient source SAX J1750.8-2900. We report the discovery of kHz QPOs in the persistent emission and of oscil-

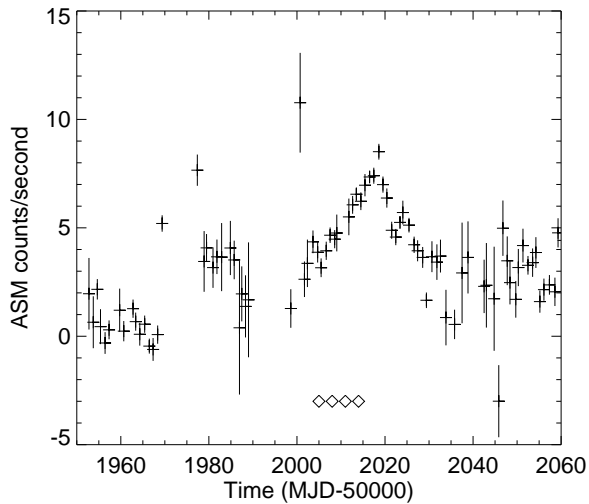


Fig. 1.— RXTE/ASM light curve of the 2001 outburst of SAX J1750.8-2900. The points are one day averages of the ASM count rates. The diamonds indicate the times of the PCA observations.

lations in one X-ray burst. We describe the source and our observations in §2, our results on X-ray bursts in §3, our results on the persistent emission in §4, and discuss our results in §5.

2. Observations of SAX J1750.8-2900

SAX J1750.8-2900 was discovered in March 1997 with the Wide Field Cameras (WFCs) on BeppoSAX as a faint and short duration transient 1°2 from the galactic center showing type-I X-ray burst activity (Bazzano et al. 1997). Analysis of data from the WFCs and the All-Sky Monitor (ASM) on RXTE shows a peak flux of 0.12 Crab (where the unit ‘Crab’ is defined as the flux of the Crab nebula in the 2-10 keV band, $\sim 2 \times 10^{-8} \text{ erg cm}^{-2} \text{ s}^{-1}$) and activity lasting approximately 3 weeks above 0.01 Crab (Natalucci et al. 1999). The WFCs detected nine type-I X-ray bursts, with peak fluxes between 0.4 and 1.0 Crab and e -folding decay times between 4 and 11 s in the 2-8 keV band. No counterparts in other wavelength regimes were identified. The type-I bursts indicate that the source is an accreting neutron star.

SAX J1750.8-2900 turned on again four years later, on 1 March 2001 (MJD 51969), as shown by observations with the RXTE All-Sky Monitor (ASM) (announced by the MIT ASM Team), the

Proportional Counter Array (C. Markwardt, private communication), and the WFCs. The ASM light curve of the 2001 outburst is shown in Fig. 1. The ASM gives relatively poor coverage near the beginning of the outburst, so detailed information is not available on the initial rise. The high rate point at MJD 52000 is from a single ASM dwell and may be due to an X-ray burst. After the initial outburst, the source flux decayed, and then rose again with an almost linear dependence of ASM count rate with time over a period of roughly 20 days to a peak flux of 0.12 Crab, nearly identical to the 1997 maximum flux. The source subsequently decayed over 10 days to a state of reduced flux, well above the level associated with quiescence in neutron star LMXBs (Asai et al. 1998).

Bursting activity was detected in the 2001 outburst with the WFCs, although not as extensively as during the 1997 outburst probably because the coverage was not as large as in 1997. Nevertheless, the WFCs detected 4 bursts in a single observation on 4 April 2001 (MJD 52003). These four bursts have peak fluxes and light curves similar to the bursts observed in 1997. Three other bursts were detected with the WFCs during the 2001 outburst, one 13 days earlier which is atypical (Natalucci et al. in preparation), one 162 days later, and one 179 days later.

The four X-ray bursts found with the WFC triggered an RXTE Target-of-Opportunity program which led to 4 observations, on 2001 April 6, 9, 12, and 15. All of our observations occurred during the second rise in flux, as indicated in Fig. 1. Data were obtained with the Proportional Counter Array (PCA) in a spectral mode (Standard 2) with 256 energy channels and 16 s time resolution, a low resolution timing mode (Standard 1) with no energy information and 0.125 s time resolution, and a high resolution timing mode (event mode) with 122 μs time resolution and 64 energy channels. In addition, burst catcher modes were used to acquire high time resolution data when the event rates exceeded the telemetry capacity of the event mode during X-ray bursts.

3. X-Ray Bursts

We used the Standard 1 data to search for X-ray bursts and found four bursts, see Table 1 and Fig. 2. We examined the spectral evolution of the

Number	Time	Peak flux
1	Apr 06 at 13:26:13	6.1 ± 0.6
2	Apr 12 at 14:20:30	6.4 ± 0.6
3	Apr 15 at 17:02:25	4.8 ± 0.5
4	Apr 15 at 18:37:08	1.0 ± 0.2

Table 1: Properties of X-Ray Bursts. The table gives the time (UTC) at the start of each burst, and the bolometric peak flux in units of $10^{-8} \text{ erg cm}^{-2} \text{ s}^{-1}$.

bursts using burst catcher or event mode data with 64 channels of energy resolution. We extracted spectra for 0.25 s or 1 s intervals using all Proportional Counter Units (PCUs) on during each burst and all layers. The fluxes were corrected for dead-time effects. The maximum deadtime correction in the brightest burst was 7%. In order to eliminate the contribution of the persistent emission, we subtracted off a spectrum from 10 s of data preceding each burst, and fit the resulting spectra in the 3-20 keV band with an absorbed blackbody model with the column density fixed to the average value found from the persistent emission spectra described below.

The first three bursts are similar with comparable peak fluxes. The decay (e -folding) times for the full band (2–60 keV) PCA count rate for bursts 2 and 3 were close to 3.0 s. Burst 1 had a broader peak than bursts 2 and 3, had a longer decay time of 5 s, and deviated significantly from an exponential decay. Burst 4 was preceded by a small precursor event, beginning 9 s earlier with a peak count rate (with persistent emission subtracted) of $\sim 20\%$ of the main burst. Substructure including at least two small peaks is present in the precursor event. The peak count rate of burst 4 was a factor of 4 lower than the other bursts and the corresponding temperature was lower. Its decay time was 3.4 s, close to that of bursts 2 and 3.

The results of the spectral fits for the brightest burst, number 2, are shown in Fig. 3. The burst shows an increase in radius and a simultaneous decrease in temperature near the peak, but the magnitude of the radius increase is not sufficient to classify the burst as an Eddington-limited photospheric radius expansion burst. Lewin et al. (1995) found that the average peak luminosity for photospheric radius expansion bursts from

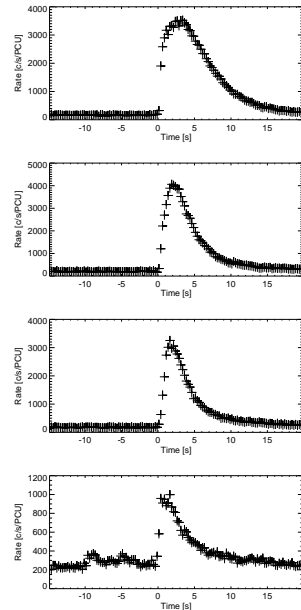


Fig. 2.— Light curves of the four bursts (burst 1 is at the top). Shown are the PCA count rates in 0.25 s intervals. The zero times are the burst start times given in Table 1

5 bursters located in globular clusters, hence with known distances, was $(3.0 \pm 0.6) \times 10^{38} \text{ erg s}^{-1}$. Using this luminosity as an upper limit on the peak luminosity in burst 2, we place an upper limit on the distance to SAX J1750.8-2900 of $6.3 \pm 0.7 \text{ kpc}$. This upper limit is consistent with the upper limit derived by Natalucci et al. (1999) of 7 kpc.

Using high time resolution data (merged event lists from the event and burst catcher modes) with no energy selection, we computed power spectra for overlapping 4 s intervals of data, with 0.125 s between the starts of successive intervals, and searched for excess power in the range 200–1200 Hz. We found oscillations in the second burst with a maximum Leahy normalized power of 49.3 at a frequency of 600.75 Hz, occurring in the burst decay 5 s after the burst rise. Allowing 2×10^4 independent trials over the 20 s duration of the burst, the chance probability of occurrence is 4×10^{-7} , equivalent to a 5.0σ detection.

The dynamical power spectrum is shown in Fig. 4. In addition to the oscillations in the burst decay, there are oscillations present near 599.5 Hz in the initial part of the burst rise. The oscilla-

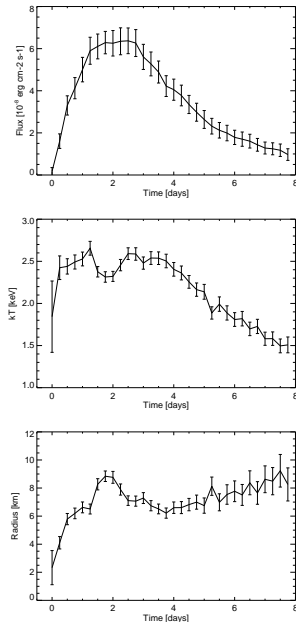


Fig. 3.— Spectral evolution of burst 2. Shown are the unabsorbed bolometric flux (top panel), the blackbody temperature (middle panel), and the equivalent radius assuming a distance of 6.3 kpc (bottom panel).

tions begin at the burst onset; no oscillations are present in the persistent emission before the burst onset. The frequency appears to change rapidly between burst rise and decay.

4. Persistent emission

To study the persistent emission, we used the Standard-2 data for spectral information and a 122 μ s time resolution event mode for timing information. We removed data around the X-ray bursts. We used only PCU 2 for the color and spectral studies as it was on during all of the observations and has a reasonably well understood response (in particular, it does not suffer from the propane layer leak experienced by PCU 0 which was the only other PCU on during all of the observations). The background estimate was made using the bright source background files and the response was calculated using pcarmf v7.10 as supplied in ftools v5.1. All PCUs on during each observation were used for the timing analysis.

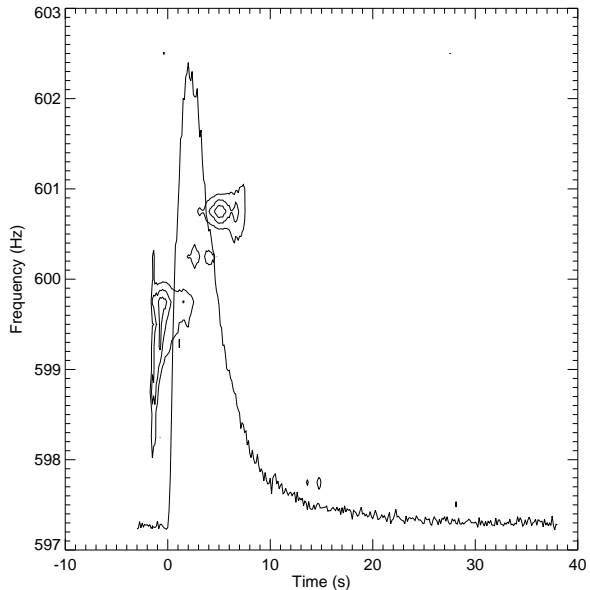


Fig. 4.— Dynamical power spectrum of burst 2 with the burst light curve (count rate) superimposed. The contours are at Leahy powers of 12, 24, and 36. The contours are generated from power spectra for overlapping 4 s intervals of data with the power plotted at the mid-point of the interval. The power apparently preceding the burst is actually due to the part of the 4 s interval overlapping the burst.

4.1. Energy spectra

We extracted an energy spectrum for each uninterrupted RXTE observing window to investigate evolution of the energy spectrum. The energy range was limited to 3-20 keV and we included a 1% systematic error. We attempted to fit the spectra with a simple absorbed powerlaw model. This was unacceptable in all cases. Addition of a gaussian emission line at an energy near the Fe-K transition produced an acceptable fit for the first spectrum, but not for the others. The sum of a blackbody plus a gaussian with absorption from material with solar abundances and the sum of a multicolor disk blackbody plus a gaussian with absorption produced unacceptable fits. The sum of a Comptonization model (Sunyaev & Titarchuk 1980) and a gaussian emission line with absorption produced acceptable fits, $\chi^2_\nu < 1$, to all of the spectra. We used this model to fit all of the persistent emission spectra. The limiting form of the Comp-

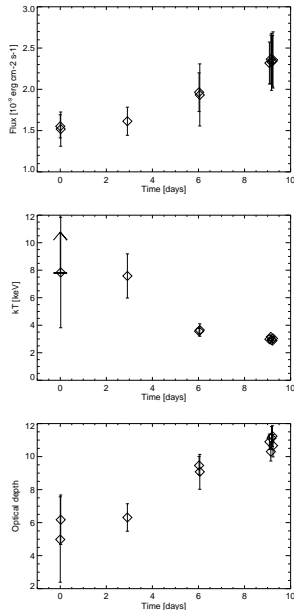


Fig. 5.— Spectral evolution of the persistent emission. Shown are the absorbed flux in the 3-20 keV band (top panel), the Comptonization temperature (middle panel), and the Comptonization optical depth (bottom panel).

tonization spectrum at high temperatures over the fitted energy band is indistinguishable from a powerlaw given our limited statistics. Therefore, only an upper limit on the Comptonization temperature could be obtained for the first observation which had a spectrum consistent with the sum of a powerlaw and emission line with absorption as noted above.

The Comptonization temperature and optical depth show marked evolution over the observations, see Fig. 5. The temperature begins high, the lower limit on the temperature in the first observation is 8 keV, and decreases to 3 keV. Simultaneously, the optical depth begins at 6 and increases to 11 for the later observations. The column density of the absorbing material shows some evidence for a decrease with time; however, we caution that these spectra are not adequate to robustly constrain the column density. The average equivalent Hydrogen column density is $4.4 \times 10^{22} \text{ cm}^{-2}$.

The iron line parameters remain roughly constant across all the observations but are poorly constrained. All of the spectra were consistent

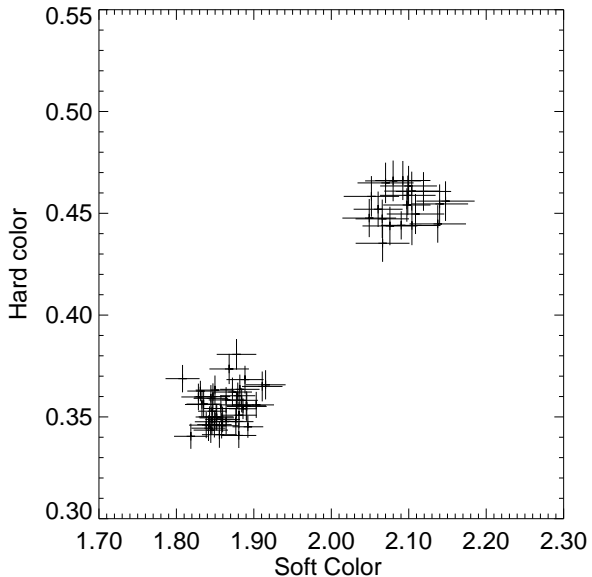


Fig. 6.— Color-color diagram of the persistent emission. Each point represents 256 s of data. The hard color is defined as the count rate in the 9.7–16 keV band divided that in the 6.4–9.7 keV band; the soft color is the 4-6.4 keV band rate divided by the 2.6–4.0 keV band rate.

with a centroid energy of 6.7 keV and this centroid energy was subsequently fixed for all of the fits. The width and normalization were allowed to vary. The best fit line widths were in the range 0.5–1.0 keV. The best fit equivalent widths ranged from 150 to 400 eV. The line width is consistent with previous results from neutron-star LMXBs (White et al. 1986; Asai et al. 2000). The equivalent width is higher than most previously reported values for neutron-star LMXBs; the maximum equivalent width reported from ASCA is 170 eV (Asai et al. 2000).

4.2. Source state and classification

We produced a color-color diagram, see Fig. 6, using 256 s intervals extracted from background subtracted Standard-2 data to study the source state. The April 6 and 9 observations form one cluster of points in the color-color diagram with high values of the hard color, while the April 12 and 15 data form a distinct cluster with lower values of the hard color.

To further investigation the source state, we

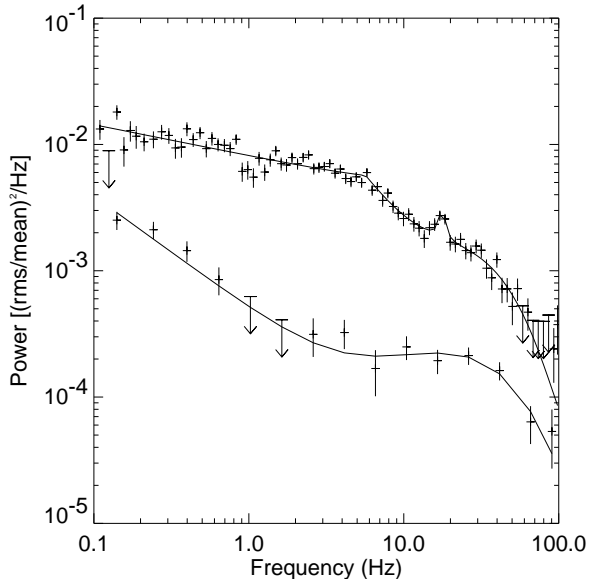


Fig. 7.— Low frequency power spectra. The upper curve is the power spectrum of the observations on April 6 and 9. The lower curve is for data from April 12 and 15. The power is RMS normalized. The solid lines are fitted curves described in the text.

produced low frequency (below 100 Hz) power spectra. We produced two spectra, one for each of the two clusters of points in the color-color diagram, see Fig. 7.

The power spectrum for the April 6 and 9 observations shows strong band-limited noise, with an RMS fraction of 12.8% in the 0.1–100 Hz range. This clearly identifies the source state as the ‘island’ state (van der Klis 1995). The power spectrum has the form of a broken powerlaw below 10 Hz and a QPO is apparent above 10 Hz. Fitting the power spectrum with the sum of a broken powerlaw plus a Lorentzian, we found excess noise above 20 Hz and $\chi^2/\text{DoF} = 143.5/75$. We added an exponentially cutoff powerlaw to fit this excess noise and the fit improved to $\chi^2/\text{DoF} = 111.8/72$. The residuals of this fit show no systematic deviations and the fit is unlikely to be improved by addition of more continuum components. For the broken powerlaw, we find a break frequency of 5.7 ± 0.2 Hz, an index below the break of -0.25 ± 0.02 and an index above the break of -1.7 ± 0.2 . The Lorentzian centroid is 17.7 ± 0.2 Hz. The break and QPO centroid

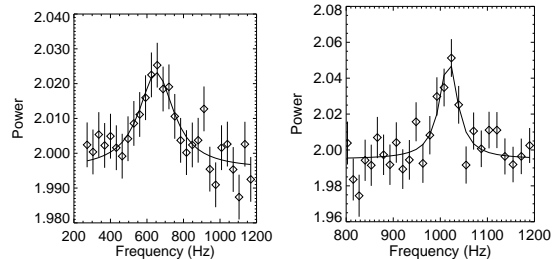


Fig. 8.— Power spectra showing kHz QPOs. The panel on the left uses data from April 9, on the right from April 12. The power spectra were calculated using events from the full PCA band (2–60 keV). The power is Leahy normalized.

frequencies are consistent with the correlation reported by Wijnands & van der Klis (1999).

The power spectrum for April 12 and 15 shows weak timing noise. The RMS fraction is 1.4% in the 0.1–100 Hz range. This indicates that the source was in the ‘banana’ state. We fitted the power spectrum with the sum of a powerlaw and an exponentially cutoff powerlaw. This gave a reasonable fit with $\chi^2/\text{DoF} = 11.6/10$. The powerlaw index was -0.89 ± 0.14 .

Based on the timing and color information, we suggest that SAX J1750.8-2900 is an atoll source. Furthermore, we identify the source as being in the “island” state on April 6 and 9, when the hard color had high values and strong timing noise was present, and in the “banana” state on April 12 and 15, when the hard color had low values and the timing noise was weak.

4.3. High frequency timing

We searched for high frequency QPOs in each uninterrupted RXTE observation window and in combinations of the various data segments. We calculated averages of 2 s power spectra for all PCA events (2–60 keV) and for events in the 4.7–20.8 keV energy band. We included events from all PCUs on during each observation. We note that the true energy band for PCU0 likely differs somewhat from the nominal range due to the propane layer leak. We searched for peaks in the spectrum and fit any peak found with a Lorentzian plus a constant equal to the calculated the Poisson noise level.

There were several QPO signals above 250 Hz,

TABLE 2
HIGH FREQUENCY PEAKS IN THE PERSISTENT EMISSION

Time (UTC)	Duration (s)	Hard color	Centroid (Hz)	Width (Hz)	Amplitude (%)
Apr 06 at 13:03:27	1344	0.46	543 ± 23	210 ± 70	8.8 ± 2.1
Apr 09 at 10:59:27	3024	0.45	651 ± 15	228 ± 45	9.5 ± 1.3
Apr 12 at 13:41:03	2336	0.37	1017 ± 4	50 ± 12	2.9 ± 0.5
Apr 15 at 14:57:35	2960	0.35	936 ± 1	8 ± 2	0.67 ± 0.13
Apr 15 all data	8608	0.35	1253 ± 9	60 ± 24	0.9 ± 0.2

NOTE.—The table includes: Time – the UTC time at the beginning of the observation, all observations were in 2001; Duration – of the observation; Hard color – as defined in Fig. 6; Centroid and Width – of the fitted Lorentzian; Amplitude – RMS fraction of QPO signal.

see Table 2. Those found on April 9 and 12 are strong detections and are shown in Fig. 8. Allowing for a number of trials equal to the search interval of 1200 Hz divided by the QPO width (van Straaten et al. 2000) and allowing several trial widths, we estimate a chance probability of occurrence of 2×10^{-11} for the QPO on April 9 and 3×10^{-6} for the QPO on April 12. These QPOs clearly establish SAX J1750.8-2900 as a new member of the class of neutron-star low-mass X-ray binaries (NS-LMXBs) exhibiting kHz QPOs. The other signals have lower significance: 2×10^{-3} for the QPO on April 6 and 2×10^{-4} for the QPO on April 15. The signal on April 15 is quite narrow and appears significant only in the 4.7-20.8 keV band power spectrum.

In addition to the signals detected in individual uninterrupted observation segments, we also found a signal at 1253 Hz in the sum of all of the April 15 data. This is the last entry in Table 2. The detection has relatively low significance and must be considered tentative. However, if the detection is correct, then the frequency difference between the two QPOs detected on April 15 is 317 Hz. The formal error on the difference of the two frequency centroids is 9 Hz. The 1253 Hz peak may be broadened due to shifts in the centroid frequency over the integration, so the true uncertainty on the dif-

ference is somewhat larger. The frequency difference is consistent with half the frequency of the burst oscillations.

5. Discussion

The results presented here establish that SAX J1750.8-2900 exhibits millisecond oscillations in its X-ray emission. The properties of the kHz QPOs in the persistent emission from SAX J1750.8-2900 are similar to those of the other neutron-star LMXB kHz QPO sources in terms of the observed frequency range and the oscillation amplitudes. Additional measurements of SAX J1750.8-2900 would be of interest to confirm our tentative detection of the second kHz QPO branch and obtain a simultaneous measurement of the kHz QPO frequency difference.

The properties of the burst oscillations from SAX J1750.8-2900 are also similar to those observed from other sources. The frequency shift seen in the single burst from SAX J1750.8-2900 exhibiting oscillations is compatible with those seen from several other sources and smaller than the large shift (by 1.32%) seen from 4U 1916-053 (Galloway et al. 2001).

X-ray burst oscillation sources appear to form two distinct classes: “fast oscillators” showing

burst oscillations near 600 Hz with the precise frequency close to twice the frequency difference of the kHz QPOs seen in the persistent emission, and “slow oscillators” showing burst oscillations near 300 Hz with the precise frequency near the difference of the kHz QPO frequencies (White & Zhang 1997). Our discovery of 600.75 Hz oscillations from SAX J1750.8-2900 establish that it is a member of the class of fast X-ray burst oscillators. Our tentative detection of two contemporaneous kHz QPOs with a frequency difference near 300 Hz is consistent with the properties of the other fast oscillators, but should be tested with additional observations.

Muno et al. (2001) showed that the fast oscillators produce burst oscillations predominately, but not exclusively, in photospheric radius expansion bursts, while the slow oscillators have oscillations in bursts both with and without photospheric radius expansion. The burst from SAX J1750.8-2900 in which we find oscillations shows weak, at best, evidence for photospheric radius expansion; in particular, it does not meet the requirement of 20 km of radius expansion of Muno et al. (2001). However, since we have a sample of only one burst with oscillations, our results are not inconsistent with those of Muno et al. (2001).

The fact that the behavior of the fast versus slow oscillators is different in regards to the occurrence of oscillations versus burst type (radius expansion or not) implies that the difference between the two classes is not an observational selection effect, i.e. due to the inclination of the neutron star spin axis relative to our line of sight, but rather a physical difference in the properties of the neutron stars (Muno et al. 2001). It would be of great interest to identify a model of the X-ray burst oscillations which explained both the large frequency shifts seen in some bursts (Galloway et al. 2001) and the dichotomy between the fast versus slow oscillators.

We greatly appreciate the assistance by the duty scientists of the BeppoSAX Science Operations Center in the near to real-time WFC data analysis. We gratefully acknowledge the efforts of the RXTE team, particularly Jean Swank and Evan Smith, in performing these target of opportunity observations. PK thanks Mal Ruderman for useful discussions and acknowledges support

from NASA grants NAG5-7405, NAG5-9097, and NAG5-9104. JZ acknowledges financial support from the Netherlands Organization for Scientific Research (NWO).

REFERENCES

- Alpar, M. A. & Shaham, J. 1985, *Nature*, 316, 239
- Asai, K., Dotani, T., Hoshi, R., Tanaka, Y., Robinson, C.R., & Terada, K. 1998, *PASJ*, 50, 611
- Asai, K., Dotani, T., Nagase, F., & Mitsuda, K. 2000, *ApJS*, 131, 571
- Bazzano, A., Heise, J., Ubertini, P., et al. 1997, *IAUC* 6597
- Bradt, H.V., Rothschild, R.E., & Swank, J.H. 1993, *A&AS*, 97, 355
- Galloway, D.K., Chakrabarty, D., Muno, M.P., & Savlov, P. 2001, *ApJ*, 549, L85
- Kaaret, P. & Ford, E.C. 1997, *Science*, 276, 1386
- Kaaret, P., Yu, W., Ford, E.C., & Zhang, S.N. 1998, *ApJ*, 497, L93
- Lewin, W.H.G., van Paradijs, J., & Taam, R.E. 1995, in *X-Ray Binaries*, ed. W.H.G. Lewin, J. van Paradijs, & E.P.J. van den Heuvel (Cambridge: Cambridge Univ. Press), 175
- Muno, M.P., Chakrabarty, D., Galloway, D.K., & Savlov, P. 2001, *ApJ*, 553, L157
- Natalucci, L., Cornelisse, R., Bazzano, A., Cocchi, M., Ubertini, P., Heise, J., In 't Zand, J.J.M., Kuulkers, E. 1999, *ApJ* 523, L45
- Sunyaev, R.A. & Titarchuk, L. 1980, *A&A*, 86, 121
- Strohmayer, T.E., Zhang, W., Swank, J.H., Smale, A., Titarchuk, L., Day, C., & Lee, U. 1996, *ApJ*, 469, L9
- Strohmayer, T.E., Zhang, W. & Swank, J.H. 1997, *ApJ*, 487, L77
- van Straaten, S., Ford, E.C., van der Klis, M., Mendez, M., & Kaaret, P. 2000, *ApJ*, 540, 1049

- van der Klis, M. 1995, in X-Ray Binaries, ed. W.H.G. Lewin, J. van Paradijs, & E.P.J. van den Heuvel (Cambridge: Cambridge Univ. Press), 252
- White, N.E., Peacock, A., Hasinger, G., Mason, K.O., Manzo, G., Taylor, B.G., & Branduardi-Raymont, G. 1986, MNRAS, 218, 129
- White, N.E. & Zhang, W. 1997, ApJ, 490, L87
- Wijnands, R. & van der Klis, M. 1999, ApJ, 514, 939